

Transformer-based Hybrid Beamforming with Dynamic Subarray for Near-Space Airship-Borne Communications

Ruiqi Wang, Zhen Gao, *Member, IEEE*, Keke Ying, Ziwei Wan, Symeon Chatzinotas, *Fellow, IEEE*, and Mohamed-Slim Alouini, *Fellow, IEEE*

Abstract—This paper proposes a hybrid beamforming framework for massive multiple-input multiple-output (MIMO) in near-space airship-borne communications. To achieve high energy efficiency (EE) in energy-constraint airships, a dynamic subarray structure is introduced, where each radio frequency chain (RFC) is connected to a disjoint subset of the antennas according to channel state information (CSI). The proposed joint dynamic hybrid beamforming network (DyHBFNet) comprises three key components: 1) An analog beamforming network (ABFNet) that optimizes the analog beamforming matrices and provides auxiliary information for the antenna selection network (ASNet) design, 2) an ASNet that dynamically optimizes the connections between antennas and RFCs, and 3) a digital beamforming network (DBFNet) that optimizes digital beamforming matrices by employing a model-driven weighted minimum mean square error algorithm for improving beamforming performance and convergence speed. The proposed ABFNet, ASNet, and DBFNet are all designed based on advanced Transformer encoders. Simulation results demonstrate that the proposed framework significantly enhances spectral efficiency and EE compared to baseline schemes. Additionally, its robust performance under imperfect CSI makes it a scalable solution for practical implementations.

Index Terms—Airship-borne communications, hybrid beamforming, MIMO-OFDM, dynamic subarray, deep learning, Transformer.

I. INTRODUCTION

Near-space airship-borne communications stand out as a promising technology in sixth-generation (6G), since near-space airships can realize extended coverage while providing lower latency due to lower altitudes (20-100 km) compared to popular low-Earth-orbit satellites [1]. To compensate for the severe path loss in long-range air-to-ground links, massive multiple-input multiple-output (MIMO) offering substantial array gain is an indispensable technique for airship-borne

The work was supported in part by the Natural Science Foundation of China under Grant 62471036, in part by Shandong Province Natural Science Foundation under Grant ZR2025QA30, in part by Beijing Natural Science Foundation under Grants L242011. (Corresponding authors: Zhen Gao and Ziwei Wan.)

Ruiqi Wang and Keke Ying are with the School of Information and Electronics, Beijing Institute of Technology, Beijing 100081, China, also with the State Key Laboratory of Environment Characteristics and Effects for Near-space, Beijing 100081, China (e-mails: rachem@126.com, ykk@bit.edu.cn).

Zhen Gao is with Beijing Institute of Technology (BIT), Zhuhai 519088, China, also with the State Key Laboratory of CNS/ATM, Beijing 100081, China, also with the Advanced Technology Research Institute, BIT, Jinan 250307, China (e-mail: gaozhen16@bit.edu.cn).

Z. Wan is with the Yangtze Delta Region Academy of Beijing Institute of Technology (Jiaxing), Jiaxing 31401 (e-mail: ziweiwan@bit.edu.cn).

Symeon Chatzinotas is with the Interdisciplinary Center for Security, Reliability and Trust (SnT) - University of Luxembourg, L-1855 Luxembourg (e-mail: Symeon.Chatzinotas@uni.lu).

M-S. Alouini is with the Computer, Electrical and Mathematical Sciences and Engineering Division, King Abdullah University of Science and Technology, Thuwal, 23955, Kingdom of Saudi Arabia (e-mail: slim.alouini@kaust.edu.sa).

communications [2]. Moreover, near-space airships are usually powered by solar panels and thus not charged frequently, which causes energy shortage for the communication tasks. This motivates the use of hybrid analog-digital (HAD) architecture [3] for near-space airship massive MIMO.

It has been reported that HAD massive MIMO with dynamic subarray structure can strike a balance between the system performance and hardware complexity [4]. In such an array architecture, the connection between the antennas and radio frequency chains (RFCs) can be adjusted according to the channel state information (CSI). To resolve the hybrid beamforming (HBF) problem under dynamic structure, an iterative algorithm based on the block coordinate descent method was proposed in [5] for single-user scenario. Furthermore, the multi-user scenario was considered in [6], where a two-stage HBF design using Butler matrices and weighted minimum mean square error (WMMSE) algorithm was proposed. However, the aforementioned methods have high computational complexity and poor adaptability, and their performance will decline significantly under imperfect CSI [7]. As a remedy, deep learning (DL)-based methods have been widely applied in the field of HBF. For example, the authors of [8] proposed a deep learning approach for joint antenna selection and HBF under dynamic structure. To avoid labeling a large amount of data during training stage, deep unsupervised learning was introduced in [9] for HBF design. However, the purely data-driven approaches fail to effectively integrate domain knowledge of conventional beamforming algorithm. Therefore, the model-driven network is a better choice for HBF. Additionally, the Transformer architecture utilizes self-attention layers integrated with a refined multi-head mechanism, demonstrating superior performance over other network models in various scenarios [10]. To the best of our knowledge, the interplay between the Transformer and the HBF under dynamic subarray structure has not been well studied.

In this paper, we propose a Transformer-based dynamic hybrid beamforming network (DyHBFNet) for HAD architecture with dynamic subarray. The proposed DyHBFNet comprises three key components:

- An analog beamforming network (ABFNet) that optimizes the analog beamforming matrices and provides auxiliary information for the subsequent antenna selection network (ASNet).
- An ASNet that utilizes the analog beamforming information provided by ABFNet to dynamically optimize the connections between antenna elements and RFCs.
- A digital beamforming network (DBFNet) that optimizes digital beamforming matrices by employing a model-driven WMMSE algorithm for improving beamforming

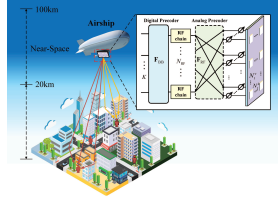


Fig. 1. Near-space airship-borne communication system assisted by HAD massive MIMO with dynamic subarray structure.

and convergence performance.

Moreover, simulation and comparative study show that the proposed scheme exhibits remarkable resilience under imperfect CSI, which makes it an excellent candidate for the beamforming design in airship-borne communications.

Notations: This paper uses lower-case letters for scalars, lower-case bold letters for column vectors, and upper-case bold letters for matrices. Superscripts $(\cdot)^*$, $(\cdot)^T$, $(\cdot)^H$, $(\cdot)^{-1}$ denote the conjugate, transpose, conjugate transpose and inversion operators, respectively. $\|\mathbf{A}\|_F$ is the Frobenius norm of \mathbf{A} and $\|\mathbf{a}\|_0$ is the l_0 norm of \mathbf{a} . $\text{vec}(\mathbf{A})$ denotes the vectorization operation. $\Re\{\cdot\}$ and $\Im\{\cdot\}$ denote the real part and imaginary part of the corresponding arguments, respectively. The (i, j) -th entry of \mathbf{A} is $[\mathbf{A}]_{i,j}$, and $[\mathbf{A}]_{i,:}([\mathbf{A}]_{:,j})$ denotes the i -th row (j -th column) of \mathbf{A} . $[\mathbf{A}]_{:,i:j}$ is the sub-matrix containing the i -th to j -th columns of \mathbf{A} . The mathematical expectation is denoted by $\mathbb{E}(\cdot)$. $\mathbf{A} \odot \mathbf{B}$ denotes the Hadamard product of \mathbf{A} and \mathbf{B} .

II. SYSTEM MODEL

We consider a downlink multi-user communication system assisted by near-space airships with HAD massive MIMO. As illustrated in Fig. 1, one aerial BS deployed at a near-space airship transmits K data streams to K single-antenna terrestrial users. The aerial BS utilizes a uniform planar array (UPA) with $N_t = N_t^v \times N_t^h$ antennas and N_{RF} RFCs, where $N_{\text{RF}} \ll N_t$, and N_t^v and N_t^h are the numbers of antennas along vertical and horizontal directions, respectively. For simplicity, we assume $N_{\text{RF}} = K$. To cope with the energy-constraint property of near-space airships, we introduce the dynamic subarray structure, i.e., each antenna is exclusively connected to a single RFC via a phase shifter (PS). We consider orthogonal frequency division multiplexing (OFDM) with N_c subcarriers. The signal received by the k -th user ($1 \leq k \leq K$) associated with the m -th subcarrier ($1 \leq m \leq N_c$) can be expressed as

$$y[k, m] = \mathbf{h}^T[k, m] \mathbf{F}_{\text{RF}} \mathbf{F}_{\text{BB}}[m] \mathbf{s}[m] + n[k, m], \quad (1)$$

where $\mathbf{h}[k, m] \in \mathbb{C}^{N_t \times 1}$ is the channel vector between the BS and the k -th user equipment (UE) associated with the m -th subcarrier, $\mathbf{F}_{\text{RF}} \in \mathbb{C}^{N_t \times K}$ is the analog beamforming matrix of the proposed dynamic subarray structure, $\mathbf{F}_{\text{BB}}[m] \in \mathbb{C}^{K \times K}$ is the baseband digital beamforming matrix, $\mathbf{s}[m] \in \mathbb{C}^{K \times 1}$ is the transmitted signal vector, which satisfies $\mathbb{E}(\mathbf{s}[m] \mathbf{s}[m]^H) = \mathbf{I}_K$, and $n[k, m] \sim \mathcal{CN}(0, \sigma_n^2)$ is additive white Gaussian noise (AWGN). Under the considered dynamic subarray structure, the analog beamforming matrix can be expressed as $\mathbf{F}_{\text{RF}} = \tilde{\mathbf{F}}_{\text{RF}} \odot \mathbf{X}_{\text{sel}}$, where $\tilde{\mathbf{F}}_{\text{RF}}$ is the analog beamforming matrix of fully-connected structure, $\mathbf{X}_{\text{sel}} \in \{0, 1\}^{N_t \times K}$ is the antenna selection matrix and each row of the matrix satisfies

$\|\mathbf{X}_{\text{sel}}\|_0 = 1$. It is worth noting that the fully-connected structure analog beamforming matrix should satisfy the unit modulus constraint, i.e., $|\tilde{\mathbf{F}}_{\text{RF}}|_{i,j} = 1/\sqrt{N_t}$. Moreover, the digital beamforming matrix should satisfy the transmit power constraint, i.e., $\|\mathbf{F}_{\text{BB}}[m]\|_F^2 = P_t$, where P_t is the transmit power allocated to each subcarrier.

III. PROPOSED JOINT DYHBFNET

In this section, we introduce the Transformer-based joint DyHBFNet. First, we characterize the channel model and formulate the corresponding optimization objective. Then, we propose the ABFNet for analog beamforming and providing auxiliary information for ASNet. Next, we develop the ASNet to design the connections between antennas and RFCs by integrating analog beamforming information to meet the requirement of dynamic subarray structure. In the end, for the DBFNet, we employ a model-driven WMMSE algorithm to improve beamforming performance and reduce computational complexity. The proposed DyHBFNet are jointly trained to maximize SE in an end-to-end manner. The block diagram of the proposed DyHBFNet is illustrated in Fig. 2.

A. Problem Formulation

Considering that the BS is deployed at a high altitude, compared with terrestrial base station communication, the channel $\mathbf{h}[k, m]$ consists of a line-of-sight (LoS) path and several non-line-of-sight (NLoS) paths, where the angles of departure (AoDs) of the NLoS paths display a small angular spread around the AoD of the LoS path. Assuming that the number of multipath components is L_p , the channel $\mathbf{h}[k, m]$ between the BS and the k -th UE associated with the m -th subcarrier can be expressed as shown in (2), where $F_k = \left(\frac{\lambda}{4\pi r_k}\right)^2$ represents the path loss with respect to large-scale fading, λ is the wavelength, r_k is the distance between the BS and the k -th UE, and $\alpha_{l,k} \sim \mathcal{CN}(0, 1)$ represents the small-scale gain of the l -th path. The azimuth and elevation angles of departure (AoDs) for the LoS path are denoted by θ_{LoS}^k and ϕ_{LoS}^k , respectively, while $\theta_{\text{NLoS}}^{l,k}$ and $\phi_{\text{NLoS}}^{l,k}$ are the azimuth and elevation AoDs of the l -th NLoS path, which are distributed around θ_{LoS}^k and ϕ_{LoS}^k with small angular spread. The relative delay of the l -th NLoS path is denoted by $\tau_{\text{NLoS}}^{l,k}$. Furthermore, $\mathbf{a}_t(\cdot)$ denotes the normalized transmit array response vector, which can be modeled as

$$\mathbf{a}_t(\theta, \phi) = [1, \dots, e^{j\frac{2\pi}{\lambda}d(m_1 \sin \theta \cos \phi + m_2 \sin \phi)}, \dots, e^{j\frac{2\pi}{\lambda}d((N_t^v - 1) \sin \theta \cos \phi + (N_t^h - 1) \sin \phi)}], \quad (3)$$

where $0 \leq m_1 \leq N_t^v - 1$, $0 \leq m_2 \leq N_t^h - 1$, and $d = \lambda/2$ is the adjacent antenna spacing.

A common optimization objective for HBF problem in airship-borne communication system is maximizing spectral efficiency (SE), which can be summarized as

$$\begin{aligned} \max_{\mathbf{F}_{\text{RF}}, \mathbf{F}_{\text{BB}}[m]} \quad & R = \frac{1}{N_c} \sum_{k=1}^K \sum_{m=1}^{N_c} \log_2(1 + \text{SINR}[k, m]) \\ \text{s.t.} \quad & \left| \tilde{\mathbf{F}}_{\text{RF}} \right|_{i,j} = \frac{1}{\sqrt{N_t}}, \forall i, j, \\ & \|\mathbf{X}_{\text{sel}}\|_0 = 1, \forall i, \|\mathbf{F}_{\text{BB}}[m]\|_F^2 = P_t, \forall m. \end{aligned} \quad (4)$$

The signal-to-interference-plus-noise ratio (SINR) of the k -th UE associated with the m -th subcarrier can be expressed as

$$\text{SINR}[k, m] = \frac{|\mathbf{h}^T[k, m] \mathbf{F}_{\text{RF}} \mathbf{f}_{\text{BB}}[k, m]|^2}{\sum_{i=1, i \neq k}^K |\mathbf{h}^T[k, m] \mathbf{F}_{\text{RF}} \mathbf{f}_{\text{BB}}[i, m]|^2 + \sigma_m^2}, \quad (5)$$

where $\mathbf{f}_{\text{BB}}[k, m] \in \mathbb{C}^{K \times 1}$ is the k -th column of $\mathbf{F}_{\text{BB}}[m]$.

B. Proposed ABFNet for Analog Beamforming

For the ABFNet, we first convert the 3-D complex-valued CSI $\mathbf{H} \in \mathbb{C}^{N_c \times K \times N_t}$ into a real-valued matrix by concatenating $\Re\{\mathbf{H}\}$ and $\Im\{\mathbf{H}\}$. This matrix is subsequently reshaped to get $\tilde{\mathbf{H}} \in \mathbb{R}^{K \times 2N_t N_c}$. Specifically, for the k -th ($k = 1, 2, \dots, K$) row of $\tilde{\mathbf{H}}$, its first $N_t N_c$ entries, i.e. $[\tilde{\mathbf{H}}]_{k, 1:N_t N_c}$, are $\text{vec}(\Re\{\mathbf{H}[k]\})$, while the next $N_t N_c$ entries are $\text{vec}(\Im\{\mathbf{H}[k]\})$. $\tilde{\mathbf{H}}$ serves as the input to Transformer Encoder 1. Here, K denotes the input sequence length for the Transformer to extract the correlation between the RFCs.

Within the Transformer, the input sequence is first mapped to a sequence of vectors with a dimension of 256 using a fully connected (FC) linear layer followed by a positional embedding layer. The positional embedding employs sine functions at different frequencies to encode the positions of different subcarriers. The Transformer then processes this sequence through three identical layers, each consisting of a multi-head self-attention sublayer and a multilayer perception sublayer to extract high-level features from the input sequence.

Then Transformer Encoder 1 generates the real and imaginary parts of $\tilde{\mathbf{F}}_{\text{RF}}$. By applying a complex function and performing amplitude normalization, the analog beamforming matrix that satisfies the unit modulus constraint is obtained. Meanwhile, the $\Re\{\tilde{\mathbf{F}}_{\text{RF}}\}$ and $\Im\{\tilde{\mathbf{F}}_{\text{RF}}\}$ are processed by an FC layer and then reshaped into $\tilde{\mathbf{F}}_{\text{RF}} \in \mathbb{R}^{N_c \times 2KN_t}$ to provide analog beamforming information for the ASNet design.

C. Proposed ASNet for Antenna Selection

The ASNet is designed to select the optimal connections between antennas and RFCs, aiming to maximizing SE under the hardware constraint of dynamic subarray structure. Given $\|[\mathbf{X}_{\text{sel}}]_{i,:}\|_0 = 1$, the design of \mathbf{X}_{sel} can be formulated as N_t multi-class classification tasks, where each of the N_t antennas is assigned to a single RFC. First, the real-valued perfect CSI is reshaped into a matrix $\hat{\mathbf{H}} \in \mathbb{R}^{N_c \times 2KN_t}$. Then, $\hat{\mathbf{H}}$ is concatenated with $\tilde{\mathbf{F}}_{\text{RF}}$ output from Transformer Encoder 1, forming a real-valued sequence of size $N_c \times 4KN_t$ as the input to Transformer Encoder 2. Here, N_c denotes the effective input sequence length. The extracted features with dimension of $N_c \times KN_t$ are then passed through a FC linear layer and reshaped to obtain the matrix $\tilde{\mathbf{X}}_{\text{sel}} \in \mathbb{R}^{N_t \times K}$. Subsequently, the softmax activation function is applied to convert $\tilde{\mathbf{X}}_{\text{sel}}$ into a probability matrix. To get the antenna selection matrix, we use the argmax function to determine the maximum value in each

row of the matrix \mathbf{X}_{sel} . More particularly, for the (i, j) -th entry of \mathbf{X}_{sel} , it equals 1 only when $j = \arg \max_j(\text{softmax}([\tilde{\mathbf{X}}_{\text{sel}}]_{i,:}))$ and remains 0 in other cases. Finally, \mathbf{F}_{RF} is obtained by the Hadamard product of $\tilde{\mathbf{F}}_{\text{RF}}$ and \mathbf{X}_{sel} .

D. Proposed DBFNet for Digital Beamforming

For the digital beamforming, we employ the low-complexity model-driven WMMSE algorithm to achieve improved beamforming performance. With the analog beamforming matrix \mathbf{F}_{RF} designed by ABFNet and ASNet, and given the CSI $\mathbf{h}[k, m]$, the BS can obtain the equivalent baseband CSI matrix as $\mathbf{h}_{\text{equ}}^T[k, m] = \mathbf{h}^T[k, m] \mathbf{F}_{\text{RF}}$. Then the optimization problem in (4) can be simplified as

$$\begin{aligned} \max_{\mathbf{F}_{\text{BB}}[m]} \quad & R = \frac{1}{N_c} \sum_{k=1}^K \sum_{m=1}^{N_c} R[k, m] \\ \text{s.t.} \quad & \|\mathbf{F}_{\text{BB}}[m]\|_F^2 = P_t, \forall m. \end{aligned} \quad (6)$$

In traditional WMMSE algorithm, it has been proved that the SE maximization problem in (6) is equivalent to a sum-mean square error minimization problem [11], and thus problem (6) can be further separated into three convex sub-problems which are solved alternatively to obtain a local optima of digital beamforming matrix. Specifically, the alternative optimization of WMMSE can be summarized as follows

$$u[k, m] = \frac{\mathbf{h}_{\text{equ}}^T[k, m] \mathbf{f}_{\text{BB}}[k, m]}{\sum_{l=1, l \neq k}^K |\mathbf{h}_{\text{equ}}^T[k, m] \mathbf{f}_{\text{BB}}[l, m]|^2 + \sigma_m^2}, \quad (7)$$

$$w[k, m] = (1 - \frac{|\mathbf{h}_{\text{equ}}^T[k, m] \mathbf{f}_{\text{BB}}[k, m]|^2}{\sum_{l=1, l \neq k}^K |\mathbf{h}_{\text{equ}}^T[k, m] \mathbf{f}_{\text{BB}}[l, m]|^2 + \sigma_m^2})^{-1}, \quad (8)$$

$$\begin{aligned} \mathbf{f}_{\text{BB}}[k, m] = & \left(\mu[m] \mathbf{I}_K + \sum_{l=1}^K w[l, m] |u[l, m]|^2 \mathbf{h}_{\text{equ}}[l, m] \right. \\ & \left. \times \mathbf{h}_{\text{equ}}^H[l, m] \right)^{-1} u[k, m] w[k, m] \mathbf{h}_{\text{equ}}[k, m], \end{aligned} \quad (9)$$

where $u[k, m]$ and $w[k, m]$ are the corresponding auxiliary factors in WMMSE algorithm. Additionally, $\mu[m]$ is a Lagrange multiplier which can be computed by algorithm in [12].

Although the traditional WMMSE algorithm can theoretically converge to a relatively good solution, it needs a large number of iterations and may have a slow convergence speed, particularly in complex scenarios such as massive MIMO systems or situations with a large number of users [12]. To this end, we propose a Transformer-based model-driven WMMSE algorithm [13] for designing $\mathbf{f}_{\text{BB}}[k, m]$, which can greatly

$$\mathbf{h}[k, m] = \sqrt{F_k} \left[\mathbf{a}_t(\theta_{\text{LoS}}^k, \phi_{\text{LoS}}^k) + \sqrt{\frac{1}{L_p} \sum_{l=1}^{L_p} \alpha_{l,k} \mathbf{a}_t(\theta_{\text{NLoS}}^{l,k}, \phi_{\text{NLoS}}^{l,k}) e^{-j \frac{2\pi m \tau_{\text{NLoS}}^{l,k}}{N_c T_s}}} \right], \quad (2)$$

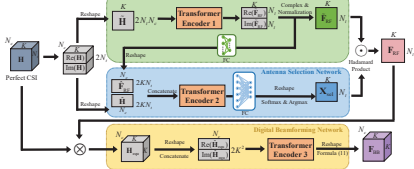


Fig. 2. Structure of the proposed joint DyHBFNet.

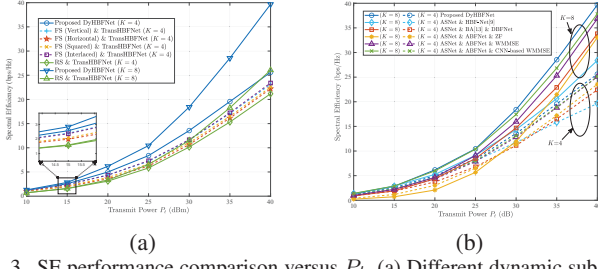


Fig. 3. SE performance comparison versus P_t . (a) Different dynamic subarray schemes with TransHBFNet. (b) ASNet with different beamforming schemes.

reduce the computational complexity. Based on (9), the optima for $\mathbf{f}_{\text{BB}}[k, m]$ takes the following form

$$\mathbf{f}_{\text{BB}}[k, m] = \left(b[m] \mathbf{I}_K + \sum_{l=1}^K c[l, m] \mathbf{h}_{\text{equ}}[l, m] \mathbf{h}_{\text{equ}}^H[l, m] \right)^{-1} \times a[k, m] \mathbf{h}_{\text{equ}}[k, m], \quad (10)$$

which indicates that the optimal digital beamforming matrix depends on parameters $\{a[k, m], b[m], c[k, m], \forall k, \forall m\}$. To obtain their value without bulky iterative algorithm, we propose a model-driven network. Specifically, Transformer Encoder 3 takes the equivalent channel $\mathbf{H}_{\text{equ}} \in \mathbb{C}^{N_c \times K \times K}$ as the input, where $\mathbf{H}_{\text{equ}}[m] = \mathbf{H}[m] \mathbf{F}_{\text{RF}}$, $m = 1, 2, \dots, N_c$. Then, we converts \mathbf{H}_{equ} into a 1D real-valued input sequence by reshaping and concatenating $\Re\{\mathbf{H}_{\text{equ}}\}$ and $\Im\{\mathbf{H}_{\text{equ}}\}$. The sequence is then processed by Transformer Encoder 3 to output the key parameters in the proposed WMMSE scheme. Formula (10) is then used to obtain the $\mathbf{F}_{\text{BB}}[m]$, $m = 1, 2, \dots, N_c$. Finally, we impose the power constraint on the digital beamforming matrix, i.e., $\mathbf{F}_{\text{BB}}[m] \leftarrow \sqrt{P_t} \frac{\mathbf{F}_{\text{BB}}[m]}{\|\mathbf{F}_{\text{BB}}[m]\|_F}$. For the proposed DyHBFNet, we choose the negative SE as the loss function, given by $L_{\text{loss}} = -\frac{1}{N_c} \sum_{k=1}^K \sum_{m=1}^{N_c} R[k, m]$.

IV. SIMULATION RESULTS

In this section, we evaluate the SE and energy efficiency (EE) performance of the proposed joint DyHBFNet.

A. Simulation Settings

In the simulations, we adopt the typical multipath MIMO-OFDM channel model described in Section II. The BS, equipped with an 8×8 UPA, serves K single-antenna UEs. The carrier frequency is $f_c = 3$ GHz, the bandwidth is $B_s = 30$ MHz, and the noise power spectral density is -174 dBm/Hz. For the LoS path of the channel, the azimuth and elevation AoD follow a uniform distribution $\mathcal{U}[-\pi/3, \pi/3]$. For the NLoS paths, the number of paths is $L_p = 30$, the path delays are uniformly distributed in $[0, 8T_s]$, where $T_s = 1/B_s$ denotes the symbol period, and the angle spread is $\Delta\theta = \pm 10^\circ$. Besides, we set $N_c = 32$, $r_k = 25$ km. The generated channel dataset is divided into

TABLE I
THE COMPARED ALGORITHMS

Abbr.	Antenna selection method	Analog beamforming method	Digital beamforming method
Proposed DyHBFNet	ASNet	ABFNet	DBFNet
FS(Vertical/Horizontal /Squared/Interfaced) [4] & TransHBFNet	FS(Vertical /Horizontal /Squared/Interfaced) [4]	ABFNet	DBFNet
RS & TransHBFNet	RS	ABFNet	DBFNet
Fully connected & TransHBFNet	Fully connected	ABFNet	DBFNet
ASNet & BA & DBFNet	ASNet	BA [13]	DBFNet
ASNet & ABFNet & ZF	ASNet	ABFNet	ZF
ASNet & ABFNet & WMMSE	ASNet	ABFNet	WMMSE
ASNet & ABFNet & CNN-based WMMSE [14]	ASNet	ABFNet	CNN-based WMMSE [14]
ASNet & HBF-Net [9]	ASNet		HBF-Net [9]
E-HBF-Net-1/2 [15]			E-HBF-Net-1/2 [15]

training, validation, and testing subsets, containing 204,800, 20,480, and 20,480 samples, respectively. The proposed neural network is implemented on a system with NVIDIA GeForce GTX 2080Ti GPU. Training is conducted with a batch size of 512 over 50 epochs, using the Adam optimizer for parameter updates. Additionally, a learning rate schedule with a warm-up strategy is applied to improve convergence efficiency.

B. Performance Comparison

To systematically evaluate the individual contributions of ASNet, ABFNet, and DBFNet to the proposed DyHBFNet, we conduct a series of ablation studies. For simplicity in subsequent discussions, ABFNet and DBFNet are collectively labeled as TransHBFNet. In Table I, we employ the ASNet, one of the four fixed selection (FS) approaches in [4], random selection (RS) approach, or fully connected approach as the antenna selection method. The ABFNet or beam alignment (BA) [13] is used as the analog beamforming method. The digital beamforming methods include the DBFNet, Zero Forcing (ZF), WMMSE and CNN-based WMMSE [14].

Additionally, in Table I, we compared TransHBFNet with HBF-Net [9] and antenna selection method with E-HBF-Net [15]. Specifically, to ensure fair comparison with E-HBF-Net [15], we adopt two approaches: E-HBF-Net-1 implements the dynamic subarray architecture in [15], which allows arbitrary connection between each antenna and RF chains, and is trained with the loss function defined in [15]. E-HBF-Net-2 only adopts the CNN structure in [15], while keeping the subarray architecture and loss function consistent with our letter.

As shown in Fig. 3(a), the proposed ASNet architecture achieves significant performance gains compared to the conventional FS and RS approaches. Fig. 3(b) shows that the ABFNet demonstrates superior performance over the BA algorithm and the DBFNet design surpasses ZF, traditional WMMSE algorithm, and CNN-based WMMSE [14]. Also, the proposed TransHBFNet performs better SE than HBF-Net [9]. Moreover, the proposed scheme demonstrates consistent performance advantages over baseline methods across varying user numbers ($K = 4$ and $K = 8$), highlighting the architecture's scalability.

Furthermore, considering that both RF components and baseband processing contribute to the overall power consumption in MIMO systems, the EE can be expressed as $\eta = \frac{R}{P_t + P_{\text{BB}} + N_{\text{RF}} P_{\text{RF}} + N_t (P_{\text{PS}} + P_{\text{SW}})}$, where $\varepsilon = 0.37$ represents the efficiency of the power amplifier, $P_{\text{BB}} = 1$ W denotes

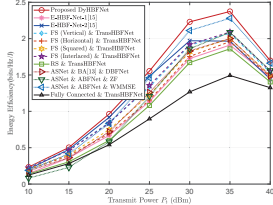


Fig. 4. EE performance comparison versus P_t .

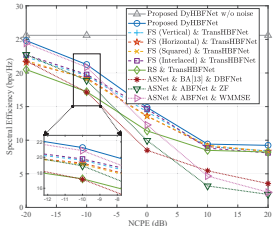


Fig. 5. SE performance comparison under imperfect CSI scenario.

TABLE II
NEURAL NETWORK COMPLEXITY COMPARISON

	Proposed DyHBFNet	E-HBF-Net-1/2 [15]	ASNet & ABFNet & CNN-based WMMSE [14]
FLOPs	133.89M	101.98M	43.48M
Parameters	18.26M	70.00M	14.54M
Runtime	11.82 ms	3.56 ms	9.56ms

the power consumption of baseband processing, and $P_{RF} = 300\text{mW}$, $P_{PS} = 40\text{mW}$, and $P_{SW} = 5\text{mW}$ are the power consumption of each RFC, PS, and switch, respectively [16]. As shown in Fig. 4, all subarray strategies exhibit superior EE compared to the fully connected strategy. Among these, the proposed DyHBFNet achieves the highest EE, demonstrating its capability to reduce energy consumption effectively.

On the other hand, the CSI in near-space communications is subject to unique perturbations induced by platform dynamics and upper atmospheric turbulence, and Fig. 5 evaluates the robustness under such imperfect CSI conditions. The normalized channel perturbation error (NCPE) is defined as $NCPE = \frac{\sum_{k=1}^K \sum_{m=1}^{N_c} \|\mathbf{h}[k, m] - \mathbf{h}_{per}[k, m]\|_2^2}{\sum_{k=1}^K \sum_{m=1}^{N_c} \|\mathbf{h}[k, m]\|_2^2}$, where the imperfect CSI matrix is modeled as $\mathbf{h}_{per}[k, m] = \mathbf{h}[k, m] + \mathbf{n}_{per}[k, m]$ and $\mathbf{n}_{per}[k, m] \sim \mathcal{CN}(0, \sigma_{per}^2)$ is the perturbation noise [17]. The proposed scheme demonstrates remarkable error resilience, as its Transformer structure effectively exploits the correlations across subcarriers to extract robust channel features from contaminated inputs.

Additionally, the network complexity of the proposed DyHBFNet and its counterparts is compared in Table II. In terms of FLOPs, the proposed DyHBFNet is higher than the other two algorithms, which can be attributed to its adoption of the more complex Transformer architecture. For parameters, the proposed DyHBFNet is lower than E-HBF-Net-1/2 but slightly higher than ASNet & ABFNet & CNN-based WMMSE [14]. This is because when extended to multi-carrier scenarios, E-HBF-Net-1/2 [15] significantly increases the parameter count of the FC layer at the final output stage to adapt to multi-carrier processing requirements. The proposed DyHBFNet has a longer runtime compared to the other algorithms, which is consistent with its higher computational complexity resulting from the Transformer architecture. Although the proposed DyHBFNet exhibits higher FLOPs and longer runtime compared to other algorithms, it achieves superior SE and EE.

V. CONCLUSION

In this paper, we proposed a Transformer-based DyHBFNet for HAD architecture with dynamic subarray in near-space airship-borne communications. The proposed network facilitates the advantages of dynamic connections between antenna elements and RFCs by three dedicated DL modules for analog beamforming, antenna selection, and digital beamforming, respectively. Extensive simulations demonstrated that the proposed scheme achieved substantial improvements in both SE and EE compared to conventional methods, especially with strong robustness against imperfect CSI.

REFERENCES

- [1] H. Liu *et al.*, "Near-space communications: The last piece of 6G space-air-ground-sea integrated network puzzle," *Space: Sci. Technol.*, vol. 5, p. 0176, Aug. 2024.
- [2] J. Heo, S. Sung, H. Lee, I. Hwang, and D. Hong, "MIMO satellite communication systems: A survey from the PHY layer perspective," *IEEE Commun. Surveys Tuts.*, vol. 25, no. 3, pp. 1543–1570, 3rd Quart., 2023.
- [3] I. Ahmed *et al.*, "A survey on hybrid beamforming techniques in 5G: Architecture and system model perspectives," *IEEE Commun. Surveys Tuts.*, vol. 20, no. 4, pp. 3060–3097, 4th Quart., 2018.
- [4] S. Park, A. Alkhateeb, and R. W. Heath, "Dynamic subarrays for hybrid precoding in wideband mmWave MIMO systems," *IEEE Trans. Wireless Commun.*, vol. 16, no. 5, pp. 2907–2920, May. 2017.
- [5] H. Li, M. Li, Q. Liu, and A. L. Swindlehurst, "Dynamic hybrid beamforming with low-resolution PSs for wideband mmWave MIMO-OFDM systems," *IEEE J. Sel. Areas Commun.*, vol. 38, no. 9, pp. 2168–2181, Sept. 2020.
- [6] C. C. Cavalcante, F. Antreich, A. L. F. de Almeida, and J. A. Nossek, "Efficient hybrid A/D beamforming for millimeter-wave systems using Butler matrices," *IEEE Trans. Wireless Commun.*, vol. 22, no. 2, pp. 1001–1013, Feb. 2023.
- [7] Y. Wang *et al.*, "Transformer-empowered 6G intelligent networks: From massive MIMO processing to semantic communication," *IEEE Wireless Commun.*, vol. 30, no. 6, pp. 127–135, Dec. 2023.
- [8] A. M. Elbir and K. V. Mishra, "Joint antenna selection and hybrid beamformer design using unquantized and quantized deep learning networks," *IEEE Trans. Wireless Commun.*, vol. 19, no. 3, pp. 1677–1688, Mar. 2020.
- [9] H. Hojatian, J. Nadal, J.-F. Frigon, and F. Leduc-Primeau, "Unsupervised deep learning for massive MIMO hybrid beamforming," *IEEE Trans. Wireless Commun.*, vol. 20, no. 11, pp. 7086–7099, Nov. 2021.
- [10] A. Vaswani *et al.*, "Attention is all you need," *Proc. Int. Conf. Adv. Neural Inf. Process. Syst. (NIPS)* (Long Beach, CA, USA), Dec. 4–9, 2017, pp. 5998–6008.
- [11] Q. Shi, M. Razaviyayn, Z.-Q. Luo, and C. He, "An iteratively weighted MMSE approach to distributed sum-utility maximization for a MIMO interfering broadcast channel," *IEEE Trans. Signal Process.*, vol. 59, no. 9, pp. 4331–4340, Sep. 2011.
- [12] Q. Hu, Y. Cai, Q. Shi, K. Xu, G. Yu, and Z. Ding, "Iterative algorithm induced deep-unfolding neural networks: Precoding design for multiuser MIMO systems," *IEEE Trans. Wireless Commun.*, vol. 20, no. 2, pp. 1394–1410, Feb. 2021.
- [13] M. Wu, Z. Gao, Y. Huang, Z. Xiao, D. W. K. Ng, and Z. Zhang, "Deep learning-based rate-splitting multiple access for reconfigurable intelligent surface-aided tera-hertz massive MIMO," *IEEE J. Sel. Areas Commun.*, vol. 41, no. 5, pp. 1431–1451, May 2023.
- [14] J. Shi, A.-A. Lu, W. Zhong, X. Gao, and G. Y. Li, "Robust WMMSE precoder with deep learning design for massive MIMO," *IEEE Trans. Commun.*, vol. 71, no. 7, pp. 3963–3976, Jul. 2023.
- [15] H. Hojatian, Z. Mlika, J. Nadal, J.-F. Frigon, and F. Leduc-Primeau, "Learning energy-efficient transmitter configurations for massive MIMO beamforming," *IEEE Trans. Mach. Learn. Commun. Netw.*, vol. 2, pp. 939–955, 2024.
- [16] R. Zhang *et al.*, "Energy efficient hybrid precoding for adaptive partially connected mmWave massive MIMO: A decomposition-based approach," *IEEE Trans. Veh. Technol.*, vol. 72, no. 12, pp. 15967–15980, Dec. 2023.
- [17] Y. Sun *et al.*, "Principal component analysis-based broadband hybrid precoding for millimeter-wave massive MIMO systems," *IEEE Trans. Wireless Commun.*, vol. 19, no. 10, pp. 6331–6346, Oct. 2020.